Antiphase boundary migration as a diffusion mechanism in a P3 sodium layered oxide

Jonas L. Kaufman and Anton Van der Ven[*]
Materials Department, University of California, Santa Barbara, Santa Barbara, California 93106, USA

The electrode materials of Na-ion batteries must exhibit fast ion transport, a property that is often negatively impacted when mobile cations order. Many layered Na (and K) intercalation compounds adopt the P3 crystal structure, which tends to stabilize cation-vacancy orderings over a wide range of Na concentrations. The ordered phases have been predicted to consist of domains that are periodically separated by antiphase boundaries (APBs) to accommodate variations in Na concentration. The mechanisms and rates with which Na diffuses within such ordered phases of P3 are not understood. We have conducted a first-principles study of Na diffusion in the P3 structure, using $Na_x CoO_2$ as a model system. We find that most simple nearest-neighbor hops in Na-vacancy ordered phases in P3 result in unstable configurations and are therefore forbidden. We identify an alternative mechanism of Na transport that is mediated by APB migration via the formation and expansion of kinks along domain boundaries. The limiting kinetic barriers for this mechanism are quite low (0.03 to 0.30 eV). Vacancy defects are not required, and furthermore have formation energies that are higher than those of the APB kink defects. Our results suggest that APB migration is a fundamental diffusion mechanism in the P3 structure.

I. INTRODUCTION

Na-ion batteries continue to attract interest as cost-effective alternatives to Li-ion batteries for select applications. In many reports, a layered transition-metal oxide intercalated with Na is used as an electrode [1–4]. Such compounds have already been widely adopted as cathodes in Li-ion batteries due to their favorable electrochemical properties [5–7]. An important criterion for evaluating cathode materials is the ease with which ions diffuse through the crystal, as the ionic conductivity of the electrodes contributes to overall rate capability of the cell [8,9]. Compared to Li, Na frequently induces more structural phase transitions and stronger ion-vacancy orderings [10–17], which can significantly affect kinetics. Many issues associated with layered oxides for Na intercalation also apply to their K analogues for the emerging K-ion batteries [18–21].

Layered oxides can adopt a variety of host crystal structures, each with distinct topologies of intercalant sites. The O3 structure [22], favored by many Li intercalation compounds such as $Li_x CoO_2$ [7,17], hosts intercalating ions in octahedral sites that form two-dimensional triangular lattices. The related O1 structure [23] also hosts intercalating ions in octahedral sites. Hops between nearest-neighbor octahedral sites of layered intercalation compounds pass through intermediate tetrahedral sites. This leads to diffusion mechanisms that are mediated by divacancies, with important consequences for the concentration dependence of the diffusion coefficient [8,23,24].

While layered Na intercalation compounds such as $Na_x CoO_2$ also favor an O3 crystal structure at high concen-

trations, they usually transform to a P3 structure upon Na extraction through a change in stacking sequence of the two-dimensional transition-metal oxide building blocks [13,22]. The P3 structure is shown in Fig. 1(a) for $Na_x CoO_2$. The Na ions of P3 occupy trigonal prismatic sites that form two-dimensional honeycomb networks. Elementary Na hops between nearest-neighbor prismatic sites in P3 pass through the shared face of their coordination prisms as illustrated in Fig. 1. Simultaneous occupation of nearest-neighbor sites in P3 is highly unfavorable due to steric repulsion [14,26]. The neighboring sites of the hop endpoints must therefore be vacant for a hop to occur as illustrated in Fig. 1(c). Second-nearest-neighbor hops are also possible in P3 if the intermediate nearest-neighbor site is unstable (Fig. S1, Ref. [27]). These crystallographic constraints lead to collective transport mechanisms that remain unexplored and poorly understood. It is generally believed that diffusion in P3 is faster than in O3 [17,28–31], but the mechanisms that are responsible for the enhanced ion mobility in P3 have not received much attention.

In this study, we investigate diffusion mechanisms in the P3 host structure from first principles, using P3-$Na_x CoO_2$ as a model. Since layered Na intercalation compounds exhibit stronger ordering tendencies than their Li counterparts [13,16], we focus in particular on the role of Na ordering in transport kinetics. Ordered phases introduce pronounced steps in the voltage profile and can impact kinetics, often reducing the mobility and/or dimensionality of transport [24,32]. Some Na and K intercalation compounds that adopt the P3 host, including $Na_x CoO_2$, are predicted to exhibit families of hierarchical phases consisting of well-ordered domains separated by a periodic array of antiphase boundaries (APBs) [16,20,21,26]. Our systematic study of diffusion in these ordered phases points to a transport mechanism that is mediated

_____
[*]avdv@ucsb.edu
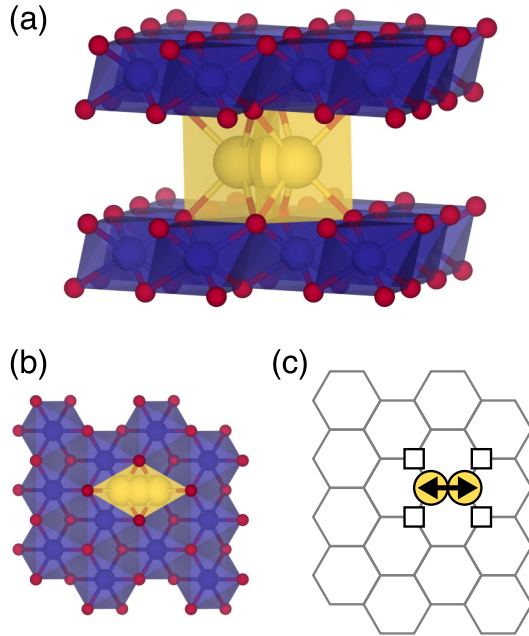
FIG. 1. (a) Side view of P3-Na$_x$CoO$_2$, with Na shown hopping between nearest-neighbor trigonal prismatic sites in the Na layer. (b) Top view of the nearest-neighbor hop. (c) The same view as (b) shown on the honeycomb network of possible Na sites. Squares indicate sites that must be vacant in order for the hop to occur. Structures visualized using VESTA [25].

FIG. 2. A section of the calculated voltage curve of Na$_x$CoO$_2$ from Ref. [26]. Experimental voltage curve taken from Ref. [12]. Insets show the in-layer Na orderings of calculated ground states at select compositions. Black lines in insets represent antiphase boundaries between regions of the $x = 1/2$ ordering.

by APB motion, as opposed to mechanisms that rely on distinct vacancies or vacancy clusters. This would make diffusion in P3 structures fundamentally different from the more conventional diffusion mechanisms of O3 and O1 hosts [8,23,24].

II. BACKGROUND

Select examples of the hierarchical orderings considered in this study are shown in Fig. 2 alongside calculated and experimentally measured voltage curves for Na$_x$CoO$_2$ [12,26]. Each step in the voltage curve corresponds to an in-layer Na ordering, with the large step at $x = 1/2$ corresponding to a particularly stable ground state that has been named ζ [26]. The local ordering is retained as the composition is decreased or increased from $x = 1/2$, with changes in composition accommodated by APBs between regions of the ζ ordering (shown as black lines in the insets of Fig. 2). There are two types of APBs: one which introduces additional vacancies and one which introduces additional Na. The average spacing between APBs can be varied nearly continuously, giving rise to a "Devil's staircase" [33,34] of orderings below and above $x = 1/2$. This description is consistent with the sloping, yet somewhat jagged structure of the measured voltage profile.

The family of orderings just below $x = 1/2$ (for $2/5 \leqslant x < 1/2$) is labeled ζ^-, while that just above $x = 1/2$ (for $1/2 < x \leqslant 4/7$) is labeled ζ^+ [26]. The average linear density of APBs is proportional to $1/2 - x$ and $x - 1/2$ for the ζ^- and ζ^+ orderings, respectively (derived in Sec. S1, Ref. [27]). The composition may equivalently be expressed in terms of the spacings between APBs, which provides a convenient way to

label specific orderings within each family. For example, the $x = 5/11$ and $x = 6/11$ orderings shown in Fig. 2 are labeled ζ_5^- and ζ_6^+, respectively [26].

The ζ^- and ζ^+ families of orderings were predicted to be stable at room temperature in Na$_x$CoO$_2$ [26]. These same intercalant orderings have also been predicted as ground states in K$_x$CoO$_2$ [20] and K$_x$CrO$_2$ [21], indicating that they are relevant in a wide range of related materials. It is therefore desirable to determine how intercalant migration occurs within such highly ordered phases. The continuous nature of these families of orderings suggests that transitions between individual phases during cycling may be accommodated by the collective motion of APBs through the crystal, but it is not immediately clear how this would occur. We seek to determine the viability of such a mechanism. We also wish to understand any differences in behavior between the "diluted" boundaries of the ζ^- orderings (those that introduce additional vacancies) and the "enriched boundaries" of the ζ^+ orderings (those that introduce additional Na). To study Na migration within these families of orderings, we chose one representative ordering from each, namely, the ζ_5^- and ζ_6^+ orderings shown in Fig. 2.

III. METHODS

First-principles calculations were performed using large periodic supercells to calculate defect energies and migration barriers within the perfectly ordered regions of the ζ ordering and in the vicinity of APBs. Supercells of the representative ζ^- and ζ^+ orderings (ζ_5^- and ζ_6^+) were chosen such that Na sites that are equidistant from an APB are symmetrically equivalent, yielding three asymmetric Na sites in each case (Fig. S3, Ref. [27]). The lowest energy stacking (under the described symmetry constraint) of each of the two primitive in-plane Na orderings was selected and tripled along the boundary direction. Finally, the c lattice vector of each supercell was adjusted to maximize the distance between each atom and its nearest periodic image in the next layer. The

resulting supercells are shown in Fig. S3 of Ref. [27]. The minimum distances between periodic image atoms in our calculations are 8.54 and 9.75 Å for the ζ^- and ζ^+ supercells, respectively. The clusters approach to statistical mechanics (CASM) software package [35–38] was used to enumerate symmetrically distinct point defects and Na hops within the chosen supercells. For all hops considered, we required that the nearest-neighbor sites of the hop endpoint sites be unoccupied to avoid steric repulsion.

Energies were calculated using the Vienna *ab initio* simulation package (VASP) [39–42]. The projector augmented wave (PAW) method [43,44] was used with the Na pv, Co, and O pseudopotentials and a plane-wave energy cutoff of 530 eV. The optB86b-vdW exchange-correlation functional [45–48] was employed to capture van der Waals interactions, as it has been shown to be effective in this system [26]. Γ-centered Monkhorst-Pack meshes [49] of density 30 Å along each reciprocal lattice vector were used to sample the Brillouin zone. Spin polarization was enabled, with all moments initialized ferromagnetically. Structures were relaxed using a force convergence criterion of 0.02 eV/Å. The representative ζ^- and ζ^+ structures were relaxed fully, but for all subsequent calculations, the lattice was fixed to the relaxed lattice of either the ζ^- or ζ^+ structure and only the ions were allowed to relax. Migration energy pathways were calculated via the nudged elastic band method as implemented in VASP, using a minimum of seven images between endpoints. Static calculations using the linear tetrahedron method [50] were performed to obtain final energies of all relaxed structures.

IV. RESULTS

We investigate defect formation and Na migration barriers in the ζ_5^- ($x = 5/11$) and ζ_6^+ ($x = 6/11$) orderings of P3-Na$_x$CoO$_2$ to determine the mechanisms with which Na diffusion occurs in the families of APB-containing P3 orderings. For brevity, we will refer to the ζ_5^- and ζ_6^+ orderings as simply ζ^- and ζ^+, respectively. Our calculations indicate that the endpoints of many Na hops within the ζ^- and ζ^+ orderings are dynamically unstable: They either relax to a different configuration or are found to reside on a local maximum of the energy surface of the crystal as revealed with NEB calculations (some examples of the latter case are shown in Fig. S4, Ref. [27]). We refer to these hops as "invalid" as their endpoints do not coincide with local minima in which the migrating Na ion can thermalize before performing a subsequent hop.

While the majority of simple nearest-neighbor hops in the ζ^- and ζ^+ orderings are found to be invalid, there are a number of allowed hops along the APBs. These valid hops are found to be crucial to Na transport as they enable a straightforward mechanism for APB migration through kink formation and lateral expansion. Our calculations predict exceedingly low migration barriers for kink formation and expansion for the ζ^- APBs, and moderately low barriers for similar pathways in the ζ^+ ordering. We also compare the defect energies required for APB migration to vacancy formation energies and determine that additional vacancies are unlikely to play a significant role in Na transport within the well-ordered ζ^- and ζ^+ phases.
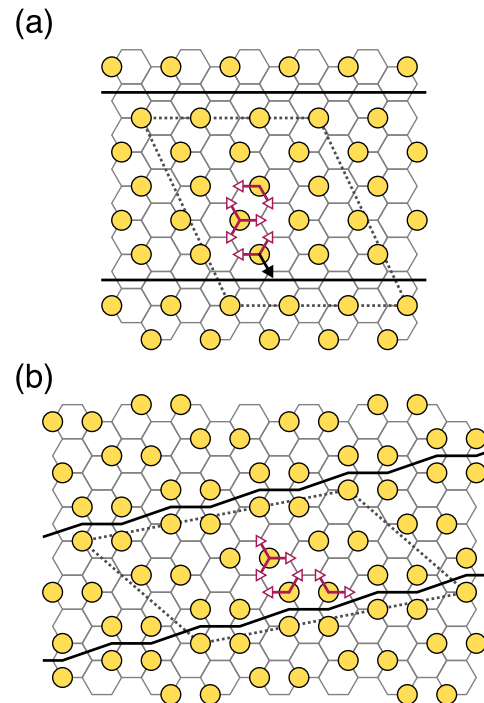
FIG. 3. Symmetrically distinct one-atom nearest-neighbor Na hops in the representative (a) ζ^- and (b) ζ^+ orderings. Dotted lines indicate the in-plane supercell. Solid black lines indicate APBs. A filled-face black arrow indicates that the hop is valid, while an open-face red arrow indicates that the hop is invalid.

A. Na migration in the perfect ζ^- and ζ^+ orderings

We enumerated all distinct one-atom first-nearest-neighbor (1A1NN) hops within the perfect ζ^- and ζ^+ orderings. These are shown in Fig. 3. Our calculations predict that almost all of these hops are invalid, indicated by open-face red arrows in Fig. 3. There is only one allowed 1A1NN hop in the ζ^- ordering and it involves the Na closest to the APB hopping towards the APB [black arrow in Fig. 3(a)]. For the ζ^+ ordering, all 1A1NN hops were found to be invalid. There are also no valid one-atom second-nearest-neighbor hops in the ζ^+ ordering, as all of them would result in a simultaneous occupation of nearest-neighbor sites.

These results demonstrate the strong resilience of the ζ ordering at $x = 1/2$ with respect antisite disorder, as the Na in regions of perfect ζ ordering between APBs in the ζ^- and ζ^+ phases are quite restricted in their mobility despite being surrounded by vacancies. In the apparent absence of simple Na migration mechanisms, we turn our attention to the possibility of collective APB migration in the ζ^- and ζ^+ orderings. This would allow for the local ζ ordering between APBs to be retained but also for vacancies/Na to move through the crystal with the APBs.

1. Boundary migration in the perfect ζ^- ordering

An examination of the lone valid 1A1NN hop in the ζ^- ordering suggests a simple mechanism for APB migration. As shown in Fig. 4, this hop forms a kink in the APB, in which a section of the boundary is translated away from the
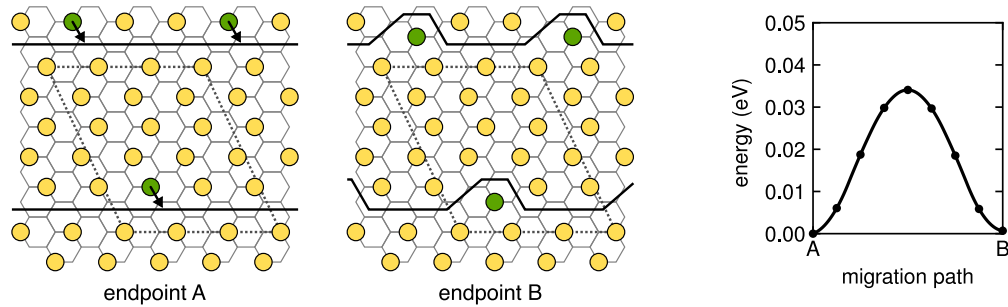
FIG. 4. Migration energy for APB kink formation in the representative ζ^- ordering. Dotted lines indicate the in-plane supercell. Solid black lines indicate APBs. Green circles indicate the hopping Na and its periodic images, with the hop direction indicated by black arrows.

rest of the boundary. The calculated migration barrier for this hop is just 0.03 eV. Furthermore, the end state of the hop has almost the same energy as the initial state, indicating that there is no defect energy associated with the kink (Fig. 4). The remarkably low migration barrier implies that kinks may form readily in the ζ^--type APBs.

Once this kind of kink has formed, it can expand via subsequent 1A1NN hops involving the Na next to the kink. As shown in Fig. 5, the kink may expand in either direction along the boundary with a migration barrier of 0.03 eV, the same as that of the initial kink formation. Note that while the kink expansion seems to introduce no additional defect energy, these hops are necessarily symmetric due to our particular choice of supercell (that is, endpoints A and B in Fig. 5 are symmetrically equivalent). This symmetry also highlights that these events may be viewed as either expansion or contraction of a kink, depending on the orientation of the kink relative to the rest of the boundary.

From simple elementary hops, we have discovered a mechanism for APB migration in the ζ^- ordering. First a kink in the boundary is formed, and then the kink can expand such that the boundary as a whole translates. The individual migration barriers required for this mechanism are very low, comparable to thermal energy at room temperature.

2. Boundary migration in the perfect ζ^+ ordering

For the perfect ζ^+ ordering, we have identified a similar mechanism to that found in the ζ^- ordering, in which kinks in the APBs may form and then expand. Although there is no 1A1NN hop possible in the perfect ζ^+ ordering, there are more complicated, two-atom hops that enable initial kink formation. Due to the orientation of the APBs, there are two distinct Na sites that lie at the boundary in the ζ^+ ordering, and there are two valid ways for these Na to collectively hop such that a kink is formed, as shown in Fig. 6. These must
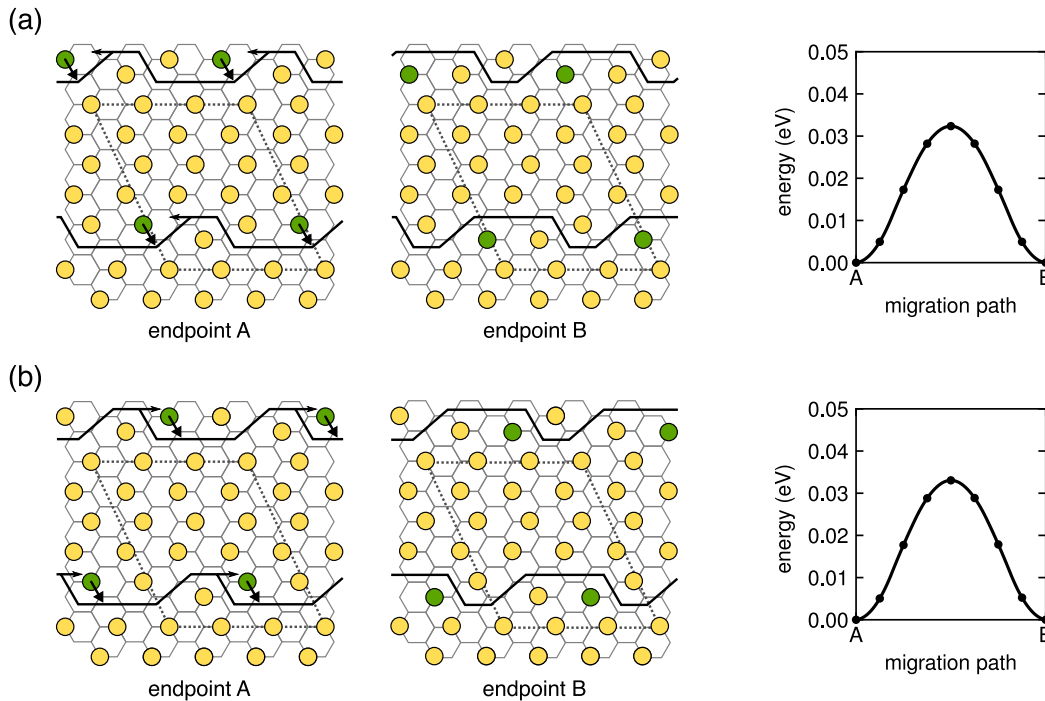
FIG. 5. Migration energies for APB kink expansion in the representative ζ^- ordering. (a) and (b) show the two possible directions for expansion from an initial kink. Dotted lines indicate the in-plane supercell. Solid black lines indicate APBs. Green circles indicate the hopping Na and its periodic images, with the hop direction and kink expansion direction indicated by black arrows.
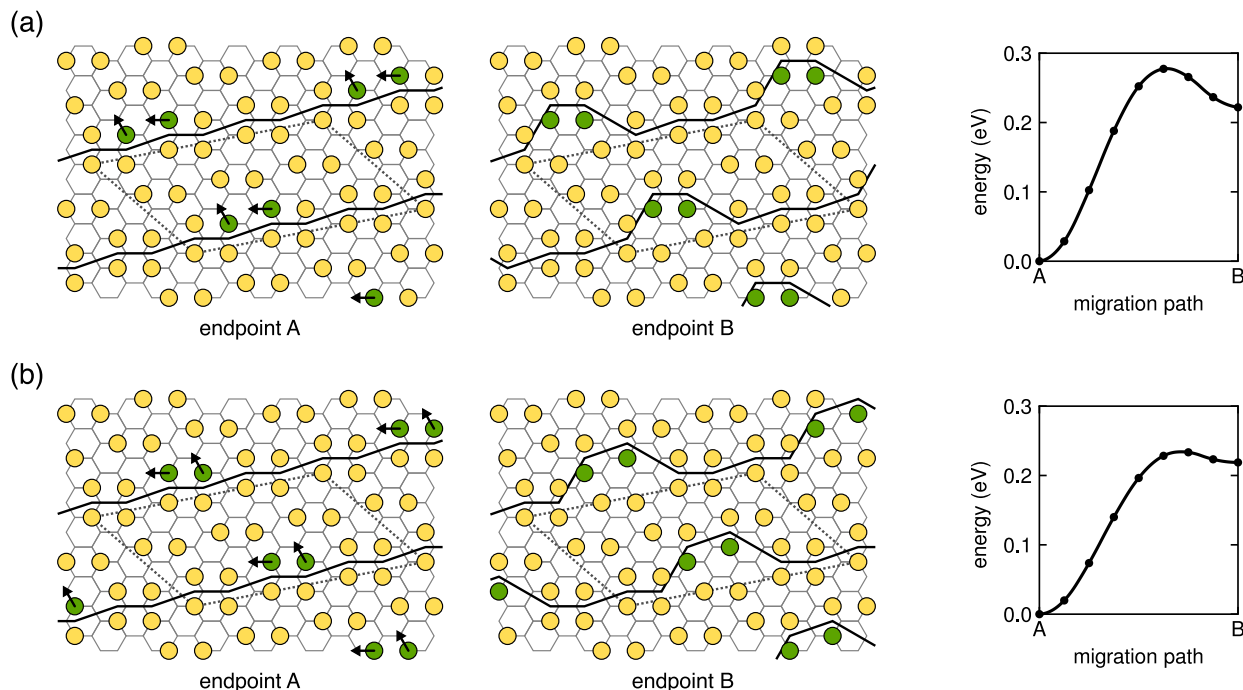
FIG. 6. Migration energies for APB kink formation in the representative ζ^+ ordering. (a) and (b) show the two types of kinks that can form. These hops occur as simultaneous two-atom hops. Dotted lines indicate the in-plane supercell. Solid black lines indicate APBs. Green circles indicate the hopping Na and their periodic images, with the hop direction indicated by black arrows.

occur as simultaneous hops, as decomposing them into pairs of valid 1A1NN hops is not possible (Fig. 3). There are two distinct types of kinks, shown forming in Figs. 6(a) and 6(b). The two types of kinks have the same defect energy of 0.22 eV, although the first type has a larger barrier to formation than the second (0.28 eV versus 0.23 eV). While these barriers are not as low as that of kink formation in the ζ^- ordering, they are still relatively low, suggesting that these kinks may readily form at room temperature.

As with the ζ^--type APBs, once a kink has formed in a ζ^+-type APB it may expand via hops involving the Na next to the kink. For example, the first type of kink [shown forming in Fig. 6(a)] may expand in either direction through 1A1NN hops, as shown in Fig. 7. Expansion in either direction requires pairs of 1A1NN hops that occur one after the other. For expansion in one direction [Fig. 7(a)], the two hops have comparable barriers (0.04 and 0.05 eV), while for expansion in the other direction [Fig. 7(b)], the first hop has a very low barrier and the second hop has a higher one (0.02 and 0.10 eV). Note that in our chosen supercell, the second type of kink [shown forming in Fig. 6(b)], is equivalent to endpoint C in Fig. 7, so that type of kink may expand by the reverse of the hops shown in Fig. 7. For completeness, this is illustrated in Fig. S5 in Ref. [27].

For the ζ^+-type APBs, all barriers for kink expansion hops are less than half of the barriers for kink formation. The defect energy for kink expansion is also negligible, as the migration barriers shown in Fig. 7 are close to symmetric. This suggests that for the ζ^+ ordering, kink formation is the limiting step in the APB migration mechanism, as once a kink has formed its expansion is relatively facile. The fact that the individual migration barriers for 1A1NN ζ^+ kink expansion hops are

nearly symmetric is consistent with the symmetry of the local environments of these hops under reversal of the hop direction, as shown in Fig. S6 in Ref. [27]. The same symmetry of the local environment does not exist for the equivalent 1A1NN hops occurring at perfect boundaries (i.e., one-atom kink formation hops), so in these cases one hop endpoint is preferred (Fig. S6, Ref. [27]). This symmetrization of the local environment may explain why 1A1NN hops at perfect ζ^+ boundaries are invalid but become valid in the presence of a kink.

B. Vacancy formation

The ζ^- and ζ^+ orderings have compositions close to $x = 1/2$ and therefore contain high concentrations of vacancies. To assess the relevance of *additional* vacancies that may mediate diffusion processes that are distinct from those that lead to kink formation and expansion (in the absence of additional vacancies), we calculated vacancy formation energies in the ζ^- and ζ^+ orderings.

The vacancy formation energy in a particular ordered phase that is stable at a Na chemical potential μ is given by

$$E_{f,Va} = E_{Va} - E + \mu, \tag{1}$$

where E_{Va} and E are the energies with and without a single point vacancy, respectively. Each type of vacancy defect has a vacancy formation energy that is a function of μ, since the ordering into which the vacancy is introduced is stable within a finite chemical potential (i.e. voltage) window. We consider the vacancy formation energies within the μ windows that stabilize the ζ_5^- and ζ_6^+ orderings. Note that this is likely an overestimation of the actual stability window size, as there are
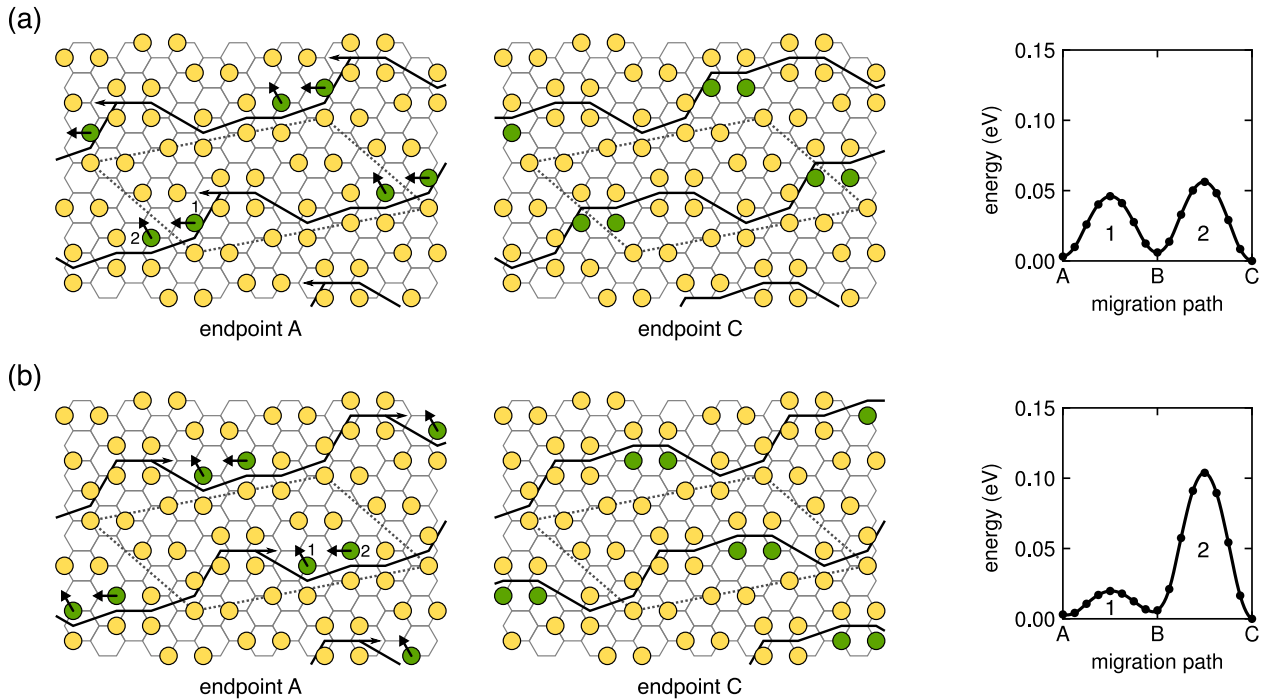
FIG. 7. Migration energies for APB kink expansion in the representative ζ^+ ordering. (a) and (b) show the two possible directions for expansion from an initial kink. These hops occur as pairs of one-atom hops, with the numbers indicating their order. Dotted lines indicate the in-plane supercell. Solid black lines indicate APBs. Green circles indicate the hopping Na and their periodic images, with the hop direction and kink expansion direction indicated by black arrows.

likely intermediate phases on the Devil's staircase of orderings that have not been explicitly included [26].

The average formation energies of point vacancies on each of the three distinct Na sites in the ζ^- and ζ^+ orderings are listed in Fig. 8, along with the energy window of each ordering. The size of the energy windows are small compared to the average vacancy formation energies, so we may use the averages as a convenient figure to discuss relative magnitudes. For the ζ^- ordering, where the boundaries are more dilute than the bulk ordering, vacancies prefer to lie away from the boundary (site 3). For the ζ^+ ordering, where the boundaries are more enriched than the bulk ordering, vacancies prefer to lie at the boundary (sites 1 and 2). This is consistent with the expectation that a homogeneous distribution of vacancies is preferred. The lowest average vacancy formation energy in the ζ^- ordering is 0.21 eV, while the lowest in the ζ^+ ordering is 0.52 eV.

We can compare these vacancy formation energies to the defect energies associated with APB migration in the ζ^- and ζ^+ orderings (Sec. IV A) to assess whether additional vacancies are likely to contribute to Na diffusion. For the ζ^- ordering, the vacancy formation energy of 0.21 eV, while low, is not negligible. In contrast, the defect energy for APB kink formation in the ζ^- ordering is essentially zero. Hence, the concentration of APB kinks should be significantly higher than the concentration of additional vacancies at room temperature in the ζ^- orderings. For the ζ^+ ordering, the defect energy associated with APB kink formation of 0.22 eV (for both types of kinks) is not insignificant, however, it is still less than half of the lowest point vacancy formation energy of 0.52 eV. As with the ζ^- ordering, the formation of APB kinks is far more favorable than the formation of vacancies in the ζ^+

ordering. We also considered combined kink-vacancy defects for the ζ^+ ordering by enumerating all distinct point vacancies in supercells containing either of the two kinks shown in Fig. 6. The lowest energy kink-vacancy defect has an average
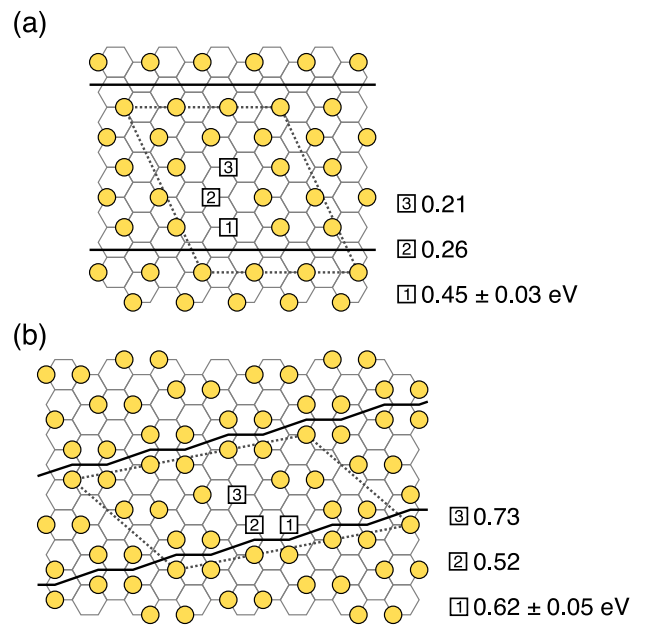
FIG. 8. Calculated formation energy windows of symmetrically distinct point vacancies in the representative (a) ζ^- and (b) ζ^+ orderings. Dotted lines indicate the in-plane supercell. Solid black lines indicate APBs. Squares indicate point vacancies on different sites, labeled by site number.

formation energy of 0.45 eV, which while lower than lowest point vacancy formation energy in the perfect ordering, is still significantly higher than the APB kink formation energy without a point vacancy. These results imply that even though additional vacancies may increase the mobility of Na in the ζ^- and ζ^+ orderings, their contribution to macroscopic Na transport is likely to be negligible in comparison to that mediated by APB migration via kink formation and expansion.

V. DISCUSSION

In this study, we have investigated Na diffusion mechanisms within highly ordered phases of P3-Na$_x$CoO$_2$. Two sets of hierarchical Na ordered phases were examined that are composed of regions of a single ordering (ζ) separated by one of two types of APBs. In the ζ^- orderings, the boundaries incorporate extra vacancies, while in the ζ^+ orderings they incorporate extra Na. The APBs are not defects, but are instead crucial features of the equilibrium phases, with the equilibrium density of APBs set by the composition x. In the perfect orderings, diffusion via simple one-atom hops appears to be quite limited, as many endpoint configurations of these hops are unstable. There are, however, valid mechanisms in both the ζ^- and ζ^+ orderings that enable the APBs themselves to migrate. This can occur by the formation of a kink in the boundary followed by the continual expansion of the kink along the boundary (much like kink-mediated processes for grain boundary motion [51,52] or surface step growth [53,54]). Additional vacancies are not only not required for this mechanism to occur, but also have defect energies that are higher than those required for APB migration.

While both the diluted APBs of the ζ^- orderings and the enriched APBs of the ζ^+ orderings allow for APB migration, the mechanisms and the energies of these processes are somewhat different. For the ζ^--type boundaries, kinks can form without incurring an energy penalty and can form and expand via one-atom hops with a minuscule barrier of 0.03 eV. These hops are low enough in energy that the motion of Na at the boundaries could serve not only as a diffusion mechanism but also as a possible source of entropy, further lowering the free energy of ζ^- phases at finite temperature. We expect the true ζ^--type APBs to be rough and dynamically shifting, unlike the perfectly straight boundaries depicted in Fig. 2. In contrast, kinks in the ζ^+-type boundaries must form via two-atom hops with barriers about an order of magnitude higher than those in the ζ^- case. Because there is also a significant kink defect energy for the ζ^+-type APBs, the reverse barriers are low, meaning it is likely that most kinks that form will subsequently be destroyed. However, kinks that persist can expand via one-atom hops that have more modest barriers than the initial kink formation. Based on these differences, we expect the ζ^+-type APBs to be both less rough (containing fewer kinks) and less mobile than the ζ^--type APBs.

In choosing a single representative from each family of APB-based orderings, we neglect any potential composition dependence of the migration barriers. To begin exploring the composition dependence of the migration barriers, we varied the c lattice parameter, which depends on composition and controls the spacing between CoO$_2$ slabs. The interslab spac-

ing is known to affect intercalant migration barriers in layered oxide systems, with larger spacings yielding lower barriers [8,23,24,55]. We recalculated formation barriers for each type of APB kink with the c lattice parameter fixed to that of the minimum or maximum composition of the corresponding family of orderings ($x = 2/5$ and $1/2$ for ζ^-, $x = 1/2$ and $4/7$ for ζ^+), using the relaxed c lattice parameters of the P3 ground state structures provided in Ref. [26]. As shown in Fig. S7 in Ref. [27], the kink formation barriers decrease with increasing c lattice parameter, as expected. However, the variation in the barriers is not large, as none of them change by more than 0.01 eV over their respective c lattice parameter ranges. While the barriers for APB migration are not strongly affected by the c lattice parameter changes induced by varying composition, there are other factors, such as in-layer electrostatic effects, that could influence the barriers more significantly as one traverses each family of orderings.

While the results of this study indicate that APB migration is an important mechanism of Na transport in well-ordered P3 phases, we acknowledge that there could be additional mechanisms that are important to diffusion. It is possible that more complicated, coordinated multi-atom hops are allowed, beyond the one- and two-atom hops considered here. Such mechanisms would likely be difficult to identify by enumeration, but could perhaps be observed in molecular dynamics simulations [32,56]. We did investigate whether the formation of APB kinks opens up any additional avenues for Na migration. For each type of APB kink, we calculated migration barriers of 1A1NN hops in the vicinity of a single kink (shown in Fig. S8 in Ref. [27], with the barriers of the valid hops listed in Table S1). As in the perfect orderings, most of the hops are invalid, but there are two valid hops for each type of kink besides the kink expansion/destruction hops discussed previously. For the ζ^- kinks, these hops have barriers that are more than double the barrier for kink expansion, while for the ζ^+ kinks, some of the additional hops have barriers comparable to those for kink expansion. This indicates that there may be additional relevant diffusion pathways in the ζ^+ orderings, but APB migration remains a significant mechanism for long-range diffusion.

Our results may have important implications for the performance of P3-Na$_x$CoO$_2$ and related electrode materials that adopt similar intercalant orderings. If APB migration is indeed the dominant diffusion mechanism, then long-range Na transport within a single crystal would be confined not just to the two-dimensional intercalation layers, but to a single dimension perpendicular to the APBs. We would also expect the Na mobility to increase with the density of APBs. This would result in a sharp drop in the diffusion coefficient as the APB density approaches zero, which occurs near $x = 1/2$. At this composition, where the ζ ordering is stable, alternative mechanisms would take over, perhaps requiring vacancy defects.

Any predictions of this study will be difficult to test experimentally without understanding the macroscopic consequences of the APB migration mechanism. While we obtain low barriers for the elementary hops required for APB migration, these may not necessarily translate to fast bulk diffusion. Rapid localized hops may be highly correlated such that back-and-forth hopping dominates. The extent to which APB

migration contributes to long-range diffusion must be determined through kinetic modeling, which could also provide estimates of effective Na diffusion coefficients and their composition dependence. However, our results reveal a subtle complication for modeling efforts in that many configurations are found to be mechanically unstable in P3. A general kinetic Monte Carlo approach using cluster expansion techniques [23,24,57–60] will likely encounter difficulties, as the unstable configurations may be erroneously visited during simulations even if the cluster expansion assigns them high formation energies. The development of a more constrained kinetic model to investigate APB migration will be the focus of a future study.

VI. CONCLUSION

We have examined diffusion mechanisms in the layered P3 crystal structure, which is adopted by many Na and K intercalation compounds at intermediate compositions. Using Na_xCoO_2 as a model system, we investigated Na migration mechanisms in phases comprised of ordered regions periodically separately by APBs. The Na in the ordered regions of these phases are largely immobile, however, atomic hops are possible along APBs, which lead to APB kink nucleation and propagation and thereby mediate Na diffusion through the crystal. This mechanism has low kinetic barriers and does not require vacancy defects. The results of this study suggest that APB migration, though distinct from conventional vacancy-mediated diffusion, is an important, if not dominant diffusion mechanism in a variety of P3 layered intercalation compounds that host APB-based ordered phases.

[1] N. Yabuuchi, K. Kubota, M. Dahbi, and S. Komaba, Research development on sodium-ion batteries, Chem. Rev. **114**, 11636 (2014).

[2] M. H. Han, E. Gonzalo, G. Singh, and T. Rojo, A comprehensive review of sodium layered oxides: Powerful cathodes for Na-ion batteries, Energy Environ. Sci. **8**, 81 (2015).

[3] C. Delmas, Sodium and sodium-ion batteries: 50 years of research, Adv. Energy Mater. **8**, 1703137 (2018).

[4] E. Goikolea, V. Palomares, S. Wang, I. R. de Larramendi, X. Guo, G. Wang, and T. Rojo, Na-ion batteries—Approaching old and new challenges, Adv. Energy Mater. **10**, 2002055 (2020).

[5] M. S. Whittingham, Lithium Batteries and Cathode Materials, Chem. Rev. **104**, 4271 (2004).

[6] M. S. Whittingham, Ultimate limits to intercalation reactions for lithium batteries, Chem. Rev. **114**, 11414 (2014).

[7] M. D. Radin, S. Hy, M. Sina, C. Fang, H. Liu, J. Vinckeviciute, M. Zhang, M. S. Whittingham, Y. S. Meng, and A. Van der Ven, Narrowing the gap between theoretical and practical capacities in Li-ion layered oxide cathode materials, Adv. Energy Mater. **7**, 1602888 (2017).

[8] A. Van der Ven, J. Bhattacharya, and A. A. Belak, Understanding Li diffusion in Li-intercalation compounds, Acc. Chem. Res. **46**, 1216 (2013).

[9] A. Van der Ven, Z. Deng, S. Banerjee, and S. P. Ong, Rechargeable alkali-ion battery materials: Theory and computation, Chem. Rev. **120**, 6977 (2020).

[10] R. Berthelot, D. Carlier, and C. Delmas, Electrochemical investigation of the P2–Na_xCoO_2 phase diagram, Nat. Mater. **10**, 74 (2011).

[11] C. Didier, M. Guignard, M. R. Suchomel, D. Carlier, J. Darriet, and C. Delmas, Thermally and electrochemically driven topotactical transformations in sodium layered oxides Na_xVO_2, Chem. Mater. **28**, 1462 (2016).

[12] K. Kubota, T. Asari, H. Yoshida, N. Yaabuuchi, H. Shiiba, M. Nakayama, and S. Komaba, Understanding the structural evolution and redox mechanism of a $NaFeO_2$–$NaCoO_2$ solid solution for sodium-ion batteries, Adv. Funct. Mater. **26**, 6047 (2016).

[13] M. D. Radin and A. Van der Ven, Stability of prismatic and octahedral coordination in layered oxides and sulfides intercalated with alkali and alkaline-earth metals, Chem. Mater. **28**, 7898 (2016).

[14] J. Vinckevičiūtė, M. D. Radin, and A. Van der Ven, Stacking-sequence changes and Na ordering in layered intercalation materials, Chem. Mater. **28**, 8640 (2016).

[15] M. D. Radin, J. Alvarado, Y. S. Meng, and A. Van der Ven, Role of crystal symmetry in the reversibility of stacking-sequence changes in layered intercalation electrodes, Nano Lett. **17**, 7789 (2017).

[16] J. L. Kaufman, J. Vinckevičiūtė, S. K. Kolli, J. G. Goiri, and A. Van der Ven, Understanding intercalation compounds for sodium-ion batteries and beyond, Philos. Trans. R. Soc. A **377**, 20190020 (2019).

[17] C. Delmas, D. Carlier, and M. Guignard, The layered oxides in lithium and sodium-ion batteries: A solid-state chemistry approach, Adv. Energy Mater. **11**, 2001201 (2020).

[18] H. Kim, J. C. Kim, M. Bianchini, D.-H. Seo, J. Rodriguez-Garcia, and G. Ceder, Recent progress and perspective in electrode materials for K-ion batteries, Adv. Energy Mater. **8**, 1702384 (2018).

[19] T. Hosaka, K. Kubota, A. S. Hameed, and S. Komaba, Research development on K-ion batteries, Chem. Rev. **120**, 6358 (2020).

[20] M. Y. Toriyama, J. L. Kaufman, and A. Van der Ven, Potassium ordering and structural phase stability in layered K_xCoO_2, ACS Appl. Energy Mater. **2**, 2629 (2019).

[21] J. L. Kaufman and A. Van der Ven, Ordering and structural transformations in layered K_xCrO_2 for K-ion batteries, Chem. Mater. **32**, 6392 (2020).

[22] C. Delmas, J.-J. Braconnier, C. Fouassier, and P. Hagenmuller, Electrochemical intercalation of sodium in Na_xCoO_2 bronzes, Solid State Ionics **3-4**, 165 (1981).

[23] A. Van der Ven, J. C. Thomas, Q. Xu, B. Swoboda, and D. Morgan, Nondilute diffusion from first principles: Li diffusion in Li_xTiS_2, Phys. Rev. B **78**, 104306 (2008).

[24] A. Van der Ven, G. Ceder, M. Asta, and P. D. Tepesch, First-principles theory of ionic diffusion with nondilute carriers, Phys. Rev. B **64**, 184307 (2001).

[25] K. Momma and F. Izumi, VESTA 3 for three-dimensional visualization of crystal, volumetric and morphology data, J. Appl. Crystallogr. **44**, 1272 (2011).

[26] J. L. Kaufman and A. Van der Ven, Na_xCoO_2 phase stability and hierarchical orderings in the O3/P3 structure family, Phys. Rev. Materials **3**, 015402 (2019).

[27] See Supplemental Material at http://link.aps.org/supplemental/10.1103/PhysRevMaterials.5.055401 for environments and energies of various hops, derivation of antiphase boundary density, supercells used for calculations, and dependence of kink formation barriers on c lattice parameter.

[28] C. Delmas, A. Maazaz, C. Fouassier, J.-M. Réau, and P. Hagenmuller, Influence de l'environnement de l'ion alcalin sur sa mobilite dans les structures a feuillets $A_x(L_xM_{1-x})O_2$, Mater. Res. Bull. **14**, 329 (1979).

[29] E. Lee, J. Lu, Y. Ren, X. Luo, X. Zhang, J. Wen, D. Miller, A. DeWahl, S. Hackney, B. Key, D. Kim, M. D. Slater, and C. S. Johnson, Layered P2/O3 intergrowth cathode: Toward high power Na-Ion batteries, Adv. Energy Mater. **4**, 1400458 (2014).

[30] B. Mortemard de Boisse, J.-H. Cheng, D. Carlier, M. Guignard, C.-J. Pan, S. Bordère, D. Filimonov, C. Drathen, E. Suard, B.-J. Hwang, A. Wattiaux, and C. Delmas, $O3–Na_xMn_{1/3}Fe_{2/3}O_2$ as a positive electrode material for Na-ion batteries: Structural evolutions and redox mechanisms upon Na^+ (de)intercalation, J. Mater. Chem. A **3**, 10976 (2015).

[31] L. Vitoux, M. Guignard, M. R. Suchomel, J. C. Pramudita, N. Sharma, and C. Delmas, The Na_xMoO_2 phase diagram (1/2 $\leqslant x < 1$): An electrochemical devil's staircase, Chem. Mater. **29**, 7243 (2017).

[32] T. J. Willis, D. G. Porter, D. J. Voneshen, S. Uthayakumar, F. Demmel, M. J. Gutmann, M. Roger, K. Refson, and J. P. Goff, Diffusion mechanism in the sodium-ion battery material sodium cobaltate, Sci. Rep. **8**, 3210 (2018).

[33] P. Bak and J. von Boehm, Ising model with solitons, phasons, and "the devil's staircase", Phys. Rev. B **21**, 5297 (1980).

[34] J. Kanamori, Infinite series of ground states of the ising model on the honeycomb lattice, J. Phys. Soc. Jpn. **53**, 250 (1984).

[35] CASM: A Clusters Approach to Statistical Mechanics, https://github.com/prisms-center/CASMcode (2020).

[36] J. C. Thomas and A. Van der Ven, Finite-temperature properties of strongly anharmonic and mechanically unstable crystal phases from first principles, Phys. Rev. B **88**, 214111 (2013).

[37] A. Van der Ven, J. Thomas, B. Puchala, and A. Natarajan, First-principles statistical mechanics of multicomponent crystals, Annu. Rev. Mater. Res. **48**, 27 (2018).

[38] B. Puchala and A. Van der Ven, Thermodynamics of the Zr-O system from first-principles calculations, Phys. Rev. B **88**, 094108 (2013).

[39] G. Kresse and J. Hafner, Ab initio molecular dynamics for liquid metals, Phys. Rev. B **47**, 558 (1993).

[40] G. Kresse and J. Hafner, Ab initio molecular-dynamics simulation of the liquid-metal–amorphous-semiconductor transition in germanium, Phys. Rev. B **49**, 14251 (1994).

[41] G. Kresse and J. Furthmüller, Efficiency of ab-initio total energy calculations for metals and semiconductors using a plane-wave basis set, Comput. Mater. Sci. **6**, 15 (1996).

[42] G. Kresse and J. Furthmüller, Efficient iterative schemes for ab initio total-energy calculations using a plane-wave basis set, Phys. Rev. B **54**, 11169 (1996).

[43] P. E. Blöchl, Projector augmented-wave method, Phys. Rev. B **50**, 17953 (1994).

[44] G. Kresse and D. Joubert, From ultrasoft pseudopotentials to the projector augmented-wave method, Phys. Rev. B **59**, 1758 (1999).

[45] J. Klimeš, D. R. Bowler, and A. Michaelides, Chemical accuracy for the van der Waals density functional, J. Phys.: Condens. Matter **22**, 022201 (2009).

[46] J. Klimeš, D. R. Bowler, and A. Michaelides, Van der Waals density functionals applied to solids, Phys. Rev. B **83**, 195131 (2011).

[47] M. Dion, H. Rydberg, E. Schröder, D. C. Langreth, and B. I. Lundqvist, Van der Waals Density Functional for General Geometries, Phys. Rev. Lett. **92**, 246401 (2004).

[48] G. Román-Pérez and J. M. Soler, Efficient Implementation of a Van der Waals Density Functional: Application to Double-Wall Carbon Nanotubes, Phys. Rev. Lett. **103**, 096102 (2009).

[49] H. J. Monkhorst and J. D. Pack, Special points for Brillouin-zone integrations, Phys. Rev. B **13**, 5188 (1976).

[50] P. E. Blöchl, O. Jepsen, and O. K. Andersen, Improved tetrahedron method for Brillouin-zone integrations, Phys. Rev. B **49**, 16223 (1994).

[51] H. Gleiter, Theory of grain boundary migration rate, Acta Metall. **17**, 853 (1969).

[52] E. Annevelink, E. Ertekin, and H. T. Johnson, Grain boundary structure and migration in graphene via the displacement shift complete lattice, Acta Mater. **166**, 67 (2019).

[53] W. K. Burton, N. Cabrera, and F. C. Frank, The growth of crystals and the equilibrium structure of their surfaces, Philos. Trans. R. Soc. London A **243**, 299 (1951).

[54] H.-C. Jeong and E. D. Williams, Steps on surfaces: Experiment and theory, Surf. Sci. Rep. **34**, 171 (1999).

[55] X. Li, Y. Wang, D. Wu, L. Liu, S.-H. Bo, and G. Ceder, Jahn–teller assisted Na diffusion for high performance Na ion batteries, Chem. Mater. **28**, 6575 (2016).

[56] Y. Mo, S. P. Ong, and G. Ceder, Insights into diffusion mechanisms in P2 layered oxide materials by first-principles calculations, Chem. Mater. **26**, 5208 (2014).

[57] J. Bhattacharya and A. Van der Ven, Phase stability and nondilute Li diffusion in spinel $Li_{1+x}Ti_2O_4$, Phys. Rev. B **81**, 104304 (2010).

[58] J. Bhattacharya and A. Van der Ven, First-principles study of competing mechanisms of nondilute Li diffusion in spinel Li_xTiS_2, Phys. Rev. B **83**, 144302 (2011).

[59] M. Aldegunde, N. Zabaras, and J. Kristensen, Quantifying uncertainties in first-principles alloy thermodynamics using cluster expansions, J. Comput. Phys. **323**, 17 (2016).

[60] J. G. Goiri, S. K. Kolli, and A. Van der Ven, Role of short- and long-range ordering on diffusion in Ni-Al alloys, Phys. Rev. Materials **3**, 093402 (2019).